Multidisciplinary investigation of a shallow near-shore landslide, Finneidfjord, Norway

Mark E. Vardy[1*], Jean-Sebastien L'Heureux[2] , Maarten Vanneste[3], Oddvar Longva[2], Alois Steiner[4], Carl Fredrik Forsberg[3], Haflidi Haflidason[5] and Jo Brendryen[5]

[1] *School of Ocean and Earth Science, University of Southampton, Southampton, UK*

[2] *Geological Survey of Norway (NGU)/International Centre for Geohazards (ICG), Trondheim, Norway*

[3] *Norwegian Geotechnical Institute (NGI)/International Centre for Geohazards (ICG), Oslo, Norway*

[4] *MARUM – Centre for Marine Environmental Sciences and Faculty of Geosciences, University of Bremen, Bremen, Germany*

[5] *Department of Earth Science, University of Bergen, Bergen, Norway*

ABSTRACT

The 1996 landslide near Finneidfjord, Norway, involved the displacement of c. 1 x 10^6 m^3 of sediment. Failure initiated offshore and developed in a retrogressive manner, back-stepping 100–150 m inland and removing a 250 m long section of the main north-south highway. The landslide caused the loss of four human lives and may have been triggered by human activity (e.g., blasting for road works and/or placement of fill along the shore). Acquisition of an extensive and multidisciplinary data set, including high-resolution swath bathymetry, 2D/3D seismic data, multiple short (up to 6 m) and two long (12 m and 14 m, respectively) sediment cores and *in situ* Free-Fall Piezocone Penetrometer (FF-CPTU) profiles complemented with geotechnical laboratory data, has provided a detailed analysis of both the landslide morphology and stratigraphic controls. Using regional 2D parametric sub-bottom profiler (TOPAS) profiles and a targeted decimetre-resolution 3D Chirp seismic volume (950 m x 140 m), we focus on post-failure material transport/deposition, correlating the failure plane against one of several regionally extensive packets of high-amplitude, composite reflections. In seismic reflection data, the slide plane lies within a distinct, thin (< 0.5 m) stratigraphic bed of lower acoustic impedance than the background sedimentation (indicated by high amplitude reverse-polarity top reflection), which is extensively deformed or completely scoured by motion of the overlying material. Within the body of the landslide, two different flow facies are identified. Inversion of these broadband (1.5–13.0 kHz) seismic data has allowed the calculation of remote physical properties (using acoustic quality factor, *Q*), affording a depth and spatial assessment of the relationship between morphology and grain size. These remote physical properties are correlated against high-resolution geotechnical data from core logs and FF-CPTU profiles, identifying the slide plane as a weak, laminated, clay-rich bed. This combined geophysical/geotechnical assessment of the landslide morphology and internal architecture supports previous work indicating a complex, multi-stage failure. These combined data illustrate how seafloor stability is strongly influenced by a shallow subsurface structure, with geotechnical properties and lateral continuity of stratified beds acting as a primary control on slide plane depth and failure probability.

INTRODUCTION

While transient factors (e.g., earthquakes, fluid flow, anthropogenic activity) are undoubtedly important, there is a growing consensus that the preconditioning of sediment prior to the trigger plays a dominant role in constraining location and area

affected by submarine landslides (Canals *et al.* 2004; Masson *et al.* 2006, 2010). Stratigraphic layers with specific soil conditions are the most widely observed preconditioning factor, as they control landslide development and extent over a large range of scales (< 1 km^3 to > 1000 km^3), in a variety of water depths (10 s metres to > km) and settings (O'Leary *et al.* 1991; Lastras *et al.* 2004; Wilson *et al.* 2004; Bryn *et al.* 2005; L'Heureux *et al.*

*mev@noc.soton.ac.uk

2010). In most of these locations, multiple failures can be correlated to a single stratigraphic layer (e.g., Lastras *et al.* 2004; Kvalstad *et al.* 2005; L'Heureux *et al.* 2010, 2012), suggesting that the layer became prone to failure at a given time and/or under certain conditions.

Understanding the morphological, lithological and geotechnical properties of these weak layers and how they precondition slope failure, is difficult. Although there have been a number of studies that have tried to characterize weak layers (e.g., Lastras *et al.* 2004; L'Heureux *et al.* 2010), a multidisciplinary investigation focusing on preconditioning, triggering and consequences, is necessary (e.g., Kvalstad *et al.* 2005; L'Heureux *et al.* 2010, 2012; Vanneste *et al.* 2012).

Here we seek to identify and quantify the soil mechanical properties of the shallow weak layer associated with the 1996 landslide near Finneidfjord, Norway, using a combined geophysical and geotechnical approach. Very high-resolution swath bathymetry and 2D seismic profiles, a decimetre-resolution 3D seismic volume, numerous short cores, two long cores and Free-Fall Piezocone Penetrometer (FF-CPTU) profiles are used to study the morphology, lithology and geotechnical properties of the weak layer. By combining the different data sets with remote physical properties inferred from very high-resolution seismic data, we are also able to position the landslide glide plane within a regionally extensive composite bed of distinct sedimentological and geotechnical properties.

REGIONAL SETTING

Sørfjorden is a 12-km long and up to 2-km wide, E-W oriented side fjord of the Ranafjord system (Fig. 1). The fjord is composed of two basins, separated by a sill/moraine ridge (Olsen *et al.* 2001). The flanks of the fjord are steep, with exposed bedrock. Beyond 200 m, the fjord bed levels out, infilled by a thick succession (up to 100 m) of Holocene marine and fluvial sediments. The eastern basin is shallower, with depths less than 60 m near the village Finneidfjord. The river-fed sediments are derived from the Røssåga River, which enters the fjord from the southeast (Fig. 1B).

The area around Sørfjorden was subject to an intense glacio-isostatic rebound and a fall in the relative sea level following
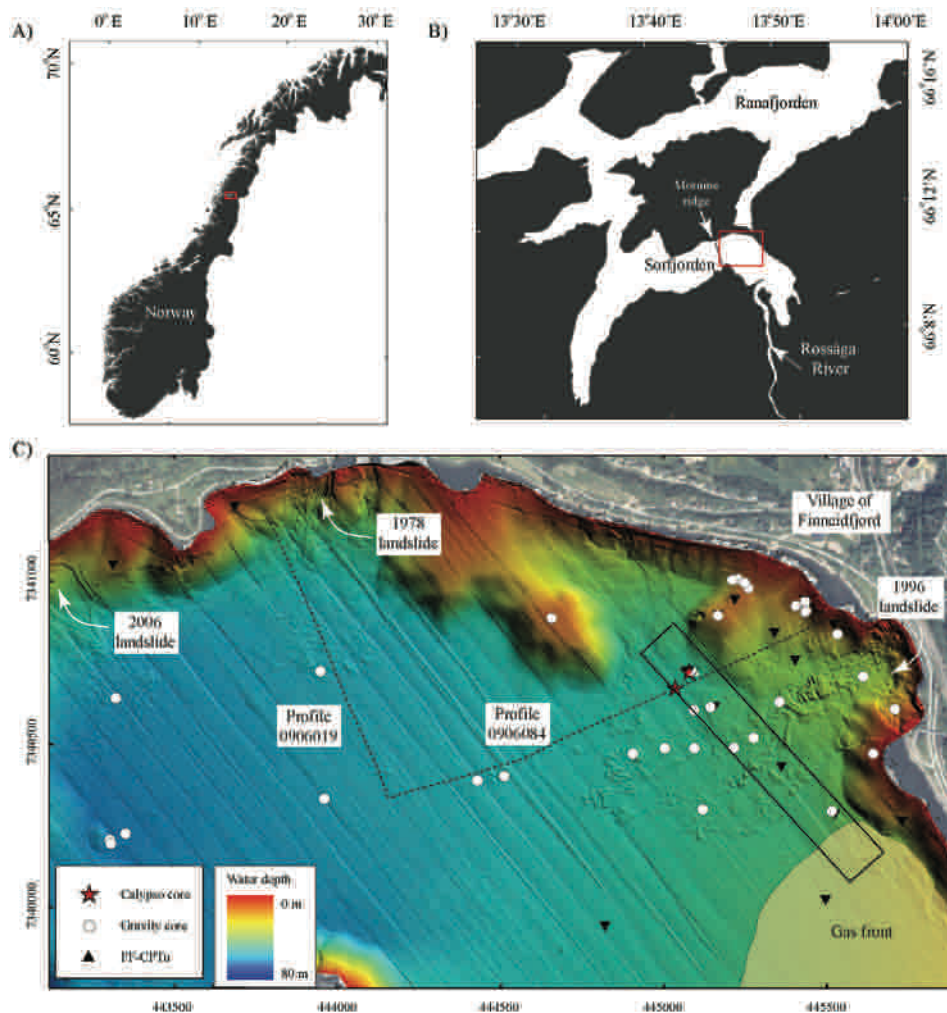

FIGURE 1

Location of the study area in Norway (A), of Sørfjorden within the Ranafjord system (B) and a GeoSwath swath bathymetry image of a larger study area illustrating the fjord bed morphology with several major landslide deposits and data discussed herein (C). Note, panel C) is projected into the UTM Zone 33N co-ordinate system. In C), the black box marks the outline of the decimetre-resolution 3D seismic volume and dashed black lines the TOPAS parametric sub-bottom profiles presented in Fig. 3.
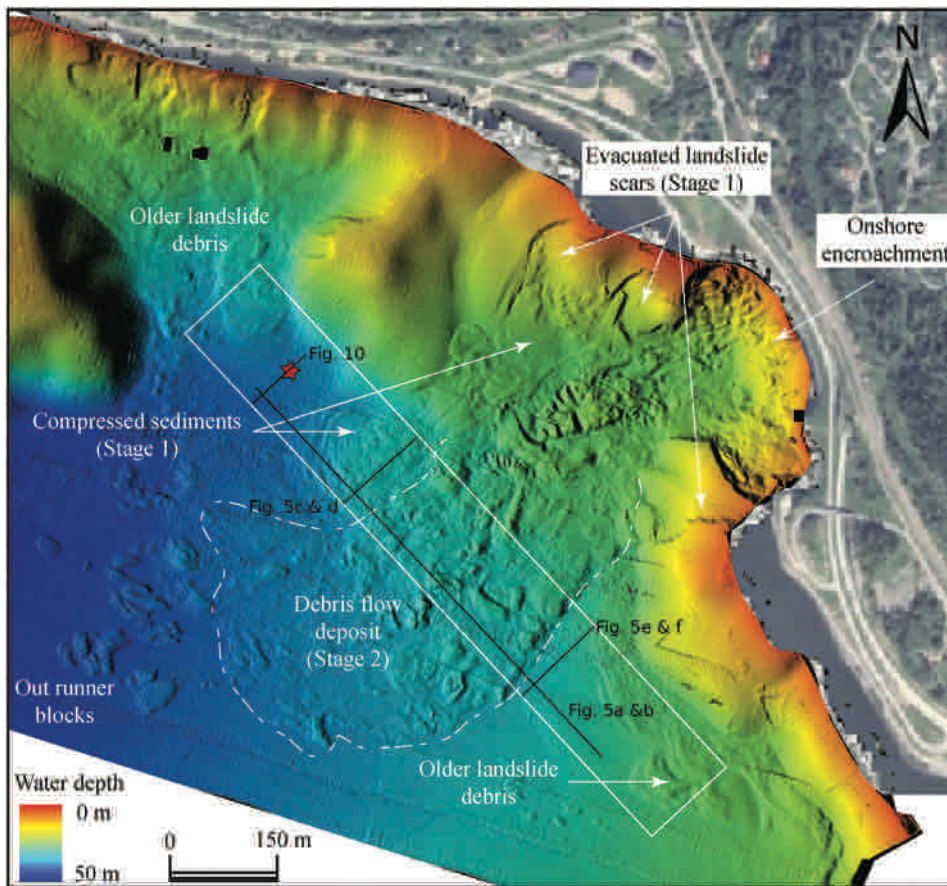
FIGURE 2

Summary of the surface morphology for the 1996 landslide imaged using high-resolution swath bathymetry (1 m bin size). The landslide stage numbering refers to the three phases of landslide development identified by Longva *et al*. (2003). The location of the decimetre-resolution 3D seismic volume and GS-10-163-01 piston core relative to the landslide deposit are indicated by a white box and red star, respectively. The black lines indicate the profiles shown in Figs 5 and 10.

deglaciation, which started in the late Preboreal period (c. 9000 ^{14}C years BP; Olsen *et al*. 2006). This uplift resulted in the sub-aerial emergence of thick glacimarine and marine deposits, lifting the marine limit to 120–128 m above the modern sea level. During their emergence in the Holocene, the marine deposits became exposed to fresh groundwater flow and the leaching of salts resulted in the development of very sensitive clays (sensitivity > 50); also called quick clays (Rosenquist 1953). Several large quick clay landslides have been triggered by river erosion in the study area during the Holocene and until the present day (Olsen *et al*. 2006; L'Heureux *et al*. 2012).

The clay-slide activity in the catchment of the fjord resulted in the deposition of regional event beds with a distinct sedimentological and geotechnical signature in the fjord stratigraphy (L'Heureux *et al*. 2012; Steiner *et al*. 2012). A combination of swath bathymetry data with high-resolution seismic data and sediment cores has shown that many of the underwater landslides in Sørfjorden initiate along these 'weak' event beds (L'Heureux *et al*. 2012). The most widely documented example being the catastrophic landslide of June 1996, which occurred just off the shoreline of the village of Finneidfjord (Fig. 2) (Longva *et al*. 2003). This relatively small landslide (1 x 10^6 m^3) initiated along a weak layer on the steep foreshore slope and, due to its retrogressive behaviour, encroached 100–150 m inland (Longva *et al*.

2003). Studies in the aftermath of the landslide suggest that several factors may have contributed to failure: excess pore pressure as a result of climatic and anthropogenic factors (e.g., blasting; Janbu 1996) or the accumulation of free gas (Best *et al*. 2003; Morgan *et al*. 2009); or an increase in overburden stress due to alongshore dumping of material (Gregersen 1999). Most recently, L'Heureux *et al*. (2012) proposed that the regional extent of the low-permeability event beds combined with periods of heavy rainfall prior to the 1996 landslide may have allowed for the formation of artesian groundwater pressure.

METHODS
Geophysical data acquisition
Overlapping swath bathymetric data sets were collected in Sørfjorden between 2003–2009. All surveys used a GeoSwath 250 kHz interferometric sonar system (GeoAcoustics Ltd) mounted onboard R/V Seisma. Attitude, tidal and water-column sound velocity corrections were applied to these data and erroneous/outlying returns removed, before binning onto a 1 m by 1 m bathymetric grid. TOPAS PS40 parametric sub-bottom profiler data were acquired at the same time as the bathymetry data. The TOPAS profiler uses 10 ms-long Chirped primary frequencies operating at 36–39 kHz and 41–44 kHz to produce a 5° wide source beam with 2–8 kHz frequency content and maximum

power at 5 kHz. In ideal cases, vertical resolution of this system is in the order of 15 cm.

These regional data are complemented by a decimetre-resolution 3D seismic volume (950 m by 140 m) targeting part of the 1996 landslide deposit, which was acquired in 2010. The University of Southampton's 3D Chirp system combines the broad bandwidth (1.5–13.0 kHz; Gutowski *et al.* 2002) and high repeatability of Chirp sub-bottom profilers with a solid array of 60 hydrophone groups to record the reflected wavefields in true 3D at decimetre-scale horizontal and vertical resolutions (Bull *et al.* 2005; Vardy *et al.* 2010, 2011).

Almost 23,000,000 traces were recorded during 4 survey days, using a shot rate of 4 pulses per second and a trace-sampling interval of 0.02 ms (i.e., 50 kHz) (box; Figs 1 and 2). Slightly over 10% of these initial traces were removed based on location outside the defined seismic volume and/or inferior signal-to-noise ratio (S/N), reducing the total number of traces contributing to the final volume to just over 20,000,000. These data were binned onto a 950 m by 140 m common midpoint (CDP) grid, with CDP spacing of 0.125 m by 0.125 m (average CDP trace fold between 4–5).

Due to the excellent raw data quality, the processing followed a simple four-step procedure:

i. Correlation with a theoretical source sweep to collapse reflections to a Klauder wavelet.
ii. Predictive deconvolution (operator = 0.15 ms; prediction length = 0.18 ms) to further compress the reflected wavelet and reduce minor ringing on higher amplitude reflections.
iii. Prestack Kirchhoff time migration into a 950 m by 140 m image space (0.125 m by 0.125 cm by 0.02 ms sampling interval) using the frequency approximated algorithm of Vardy and Henstock (2010). Migration collapses energy within a Fresnel zone, optimizing the resolution to half the receiver spacing (greater than λ/2) and strengthens the amplitudes of coherent reflections by combining energy from different shots and offsets. Due to the limited source-receiver offsets, reflector moveouts could not be used to construct a velocity model, so a constant velocity of 1500 m/s was assumed based on available water column velocity and optimal focusing of subsurface diffractions.
iv. Predictive deconvolution (operator = 0.18 ms; prediction length = 0.18 ms) to remove minor ringing on higher amplitude reflectors.

Although traditional Chirp processing involves applying an envelope function as the final processing stage to improve reflector continuity, this also reduces resolution through energy smearing and removes all phase/polarity information. We chose not to apply this processing step due to excellent data quality.

Geotechnical data acquisition

A suite of sedimentological and geotechnical data were acquired to complement the geophysical data. In 2009 a set of 12 gravity cores (up to 3 m long) were retrieved from areas within the landslide deposit, areas of exposed glide plane and from undisturbed sediments outside the area influenced by the 1996 landslide (Fig. 1). In 2010, two longer (12 and 14 m, respectively) Kullenberg-Calypso piston cores were collected using the R.V. G.O. Sars in areas of undeformed sediment immediately adjacent to the landslide deposit and within the 3D seismic volumes (Fig. 1).
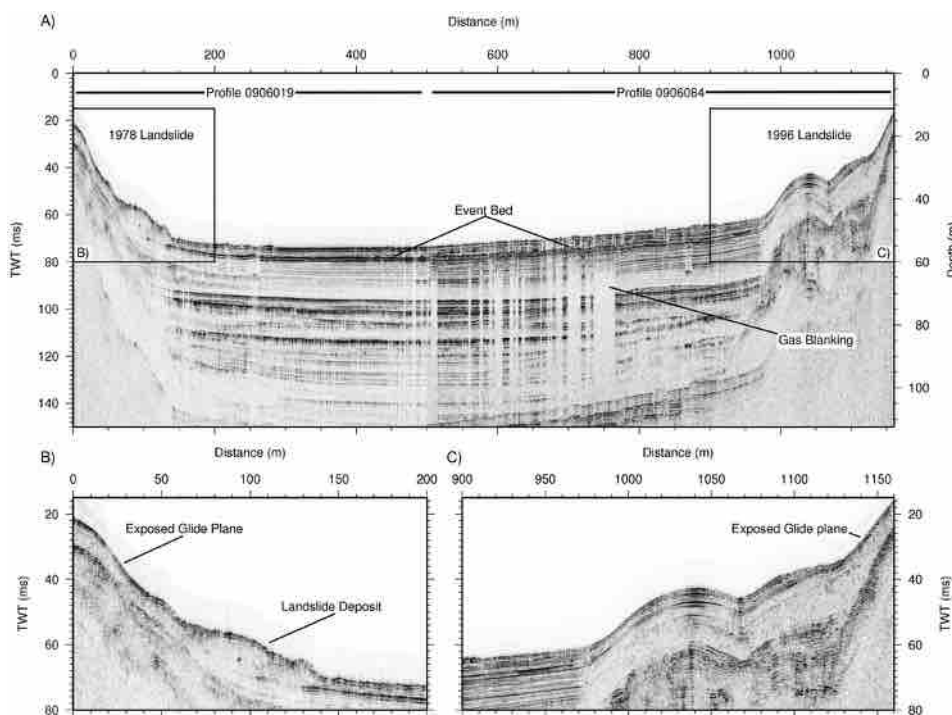

FIGURE 3
Composite section combining two crossing TOPAS parametric sub-bottom profiles (A) (for the location, see Fig. 1). Note, these data have had an envelope function applied. The packet of high-amplitude reflections c. 5 ms TWT beneath the fjord bed can be tracked underneath the landslide deposit around the break of slope on line 0906019 and becomes synonymous with the fjord bed reflection in areas of an exposed glide plane on both foreshore slopes (see insets B and C). Vertical exaggeration 1:4 for panel (A) and 1:2 for insets (B) and (C).
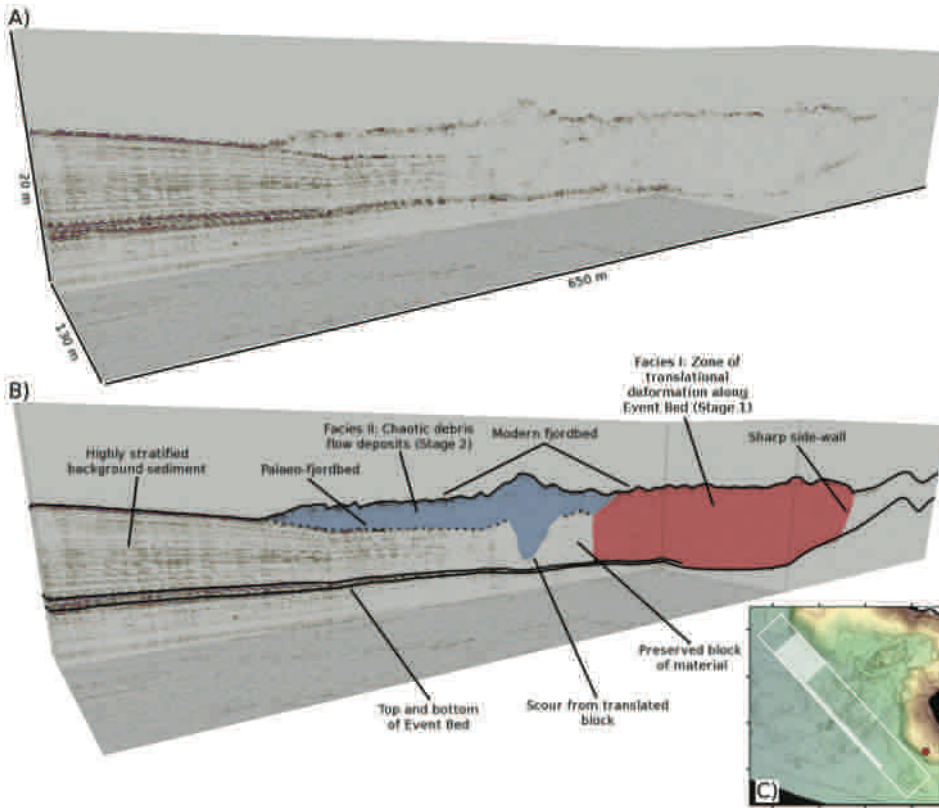
Subsequently these cores were analysed using a variety of laboratory techniques. Multi-Sensor Core Logging (MSCL, Geotek™), detailed sedimentological description and X-ray imagery were used to describe their structure, stratification and composition. These methods yield: magnetic susceptibility; density; P-wave velocity; porosity/water content; and grain size distribution.

In situ geotechnical data were acquired using MARUM's FF-CPTU (Fig. 1). A total of 38 individual drops were performed within three days, obtaining profiles for tip resistance, pore pressure response and sleeve friction, which can be used to derive undrained shear strength (s_u) and the shear strength ratio (s_u/σ'_{v0}) at a variety of locations, both in the landslide deposit and adjacent to it. A number of accelerometers and tilt meters in the housing of these equipment permit conversion from dynamic to quasi-static soil parameters (Steiner *et al*. 2012), followed by conventional CPTU processing (Lunne *et al*. 1997).

RESULTS

Geophysical evidence for a composite event bed

Swath bathymetry imaging shows evidence of mass wasting at several locations in Sørfjorden (Fig. 1). The landslide scars are generally 2–3 m high and devoid of debris, with the smooth surface in front of the scars interpreted as an exposed glide plane for these landslides. In regional TOPAS high-resolution subbottom profiles these planes correlate to a well-defined and high-amplitude reflection (Fig. 3). This high-amplitude reflection

(hitherto referred to as the event bed) is mapped throughout the whole fjord basin, from the river outlet in the south up to the moraine ridge in the deeper fjord basin.

The depth of this event bed reflection varies from c. 5 ms TWT (c. 4 m depth assuming a constant velocity of 1500 m/s) below the fjord bed in the deeper parts of the basin, to < 1 ms TWT on the foreshore slope as the sediment fill pinches out (Fig. 2). Upon detailed analysis, the wavelet is complex, sometimes becoming two clear peaks, suggesting it represents a composite reflection from a thin bed rather than an isolated impedance contrast. This event bed reflection is one of several similar high-amplitude reflections that were traced throughout the sedimentary basin, many of which coincide with the base of buried palaeo-landslide deposits (Fig. 3a) (L'Heureux *et al*. 2012).

The 1996 landslide deposit lies in the north-eastern part of the fjord, immediately south of the village of Finneidfjord. Janbu (1996), Longva *et al*. (2003) and L'Heureux *et al*. (2012) have all discussed the morphology of this deposit in some detail based on video camera trawls, swath bathymetry data and high-resolution 2D seismic profiles. They described two main failure stages. The initial phase involved translational movement of foreshore slope material on the event bed. This initial translational slide was followed by a retrogressive quick clay landslide encroaching 150 m beyond the shoreline (Fig. 2) with the liquefied material transporting large intact sediment blocks up to 2 km off the shoreline.

The same two-stage mechanism is evident in the 3D seismic volume (Fig. 4), in which the landslide deposit is divided into
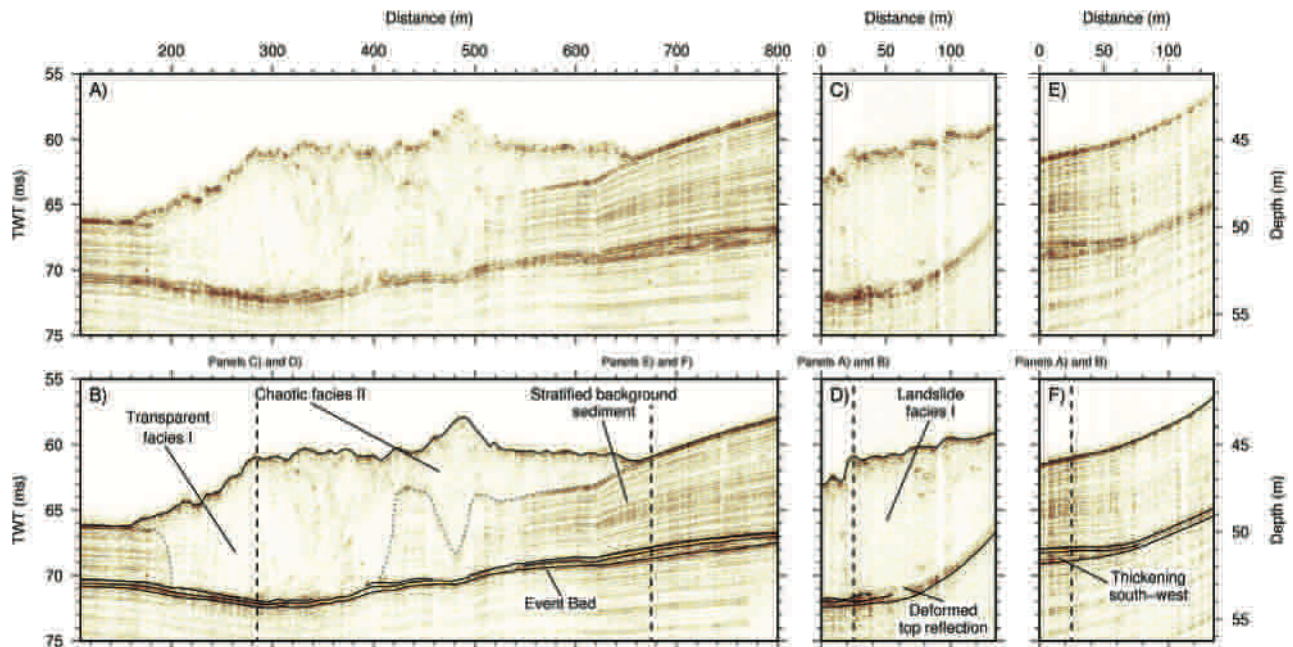
FIGURE 5

Uninterpreted (A, C, E) and interpreted (B, D, F) profiles through decimetre-resolution 3D seismic volume. Panels (A) and (B) show an in-line section illustrating how landslide facies I truncates the stratified reflections of background sediment and chaotic facies II overlays both facies I and the palaeo-fjord bed. Panels (C–F) show cross-lines through the volume, illustrating the deformation of the event bed top reflection (C and D) and thickening of the lower facies to the south-west (E and F). See Fig. 2 for locations of profiles. Vertical exaggeration 1:10.

two distinct flow facies: (I) a deeper, acoustically transparent unit, situated directly above the event bed, against which the sub-parallel reflections of the background, stratified sediment terminate; and (II) a chaotic, blocky facies that overlays both the transparent landslide facies and the palaeo-fjord bed. Although less laterally extensive (250–300 m wide), the transparent landslide facies is thicker (up to 8 ms TWT; c. 6 m), is volumetrically the larger facies (c. 150 000 m³ in the area covered by the 3D seismic data) and is interpreted as the first stage, translational failure of foreshore slope material on the event bed (Longva *et al*. 2003). The chaotic facies is much more laterally extensive (up to 500 m wide) but thinner, only locally reaching 5 ms TWT (c. 4 m) where there are large translated blocks of intact material. The better horizontal resolution of the 3D seismic data versus the high-resolution swath bathymetry (0.125 m and 1.0 m binning, respectively), allows for a much more detailed interpretation of the number and size distribution of the blocks, level of preserved internal architecture and deformation of surrounding/underlying material during block emplacement.

The slip plane associated with the translational component of this landslide correlates with the high-amplitude reflections regionally identified as the event bed on 2D TOPAS data. In the decimetre-resolution 3D seismic volume, the event bed is resolved with higher fidelity, allowing the identification of a distinct internal architecture through the identification of three key reflection horizons, which can be tracked with confidence

between core sites and across large portions of the volume (Figs 4 and 5):

i. A high-amplitude, reverse-polarity top reflection runs above the shallow gas zone in the south-eastern corner of the volume but becomes heavily deformed and/or eroded beneath the landslide deposit. The erosion of this reflector is particularly evident in the eastern (more proximal) areas of the landslide deposit, in the western (distal) part of the volume the reflector becomes identifiable, although deformed.

ii. A complex composite internal reflection of variable amplitude within the event bed that cannot be clearly resolved in the area of shallow gas and cannot be reliably tracked up the foreshore slope as the distance between top (i) and bottom (iii) reflectors diminishes. It shows significant deformation underneath the landslide immediately adjacent to the break of slope but otherwise remains identifiable even in areas where the top (i) reflection was completely removed.

iii. A normal-polarity base reflection, generally of slightly lower amplitude than top reflection (i), which is continuous over almost the whole area, only becoming unresolved in the area of shallow gas to the south-east and beneath several of the larger landslide blocks. Other than blanking beneath these blocks, the base reflection is continuous beneath the landslide, demonstrating little evidence for deformation.

These three reflections are used to subdivide the event bed into two seismic sub-facies; an upper and lower facies. Isopach maps

for these two sub-facies (Fig. 6) show a significant amount of structure. Outside the area of the landslide deposit the upper facies is consistently c. 20 cm thick. In contrast, the lower facies is highly variable, thinning significantly to below seismic resolution at the break of slope and thickening from c. 15 cm to 50 cm towards the south-west.
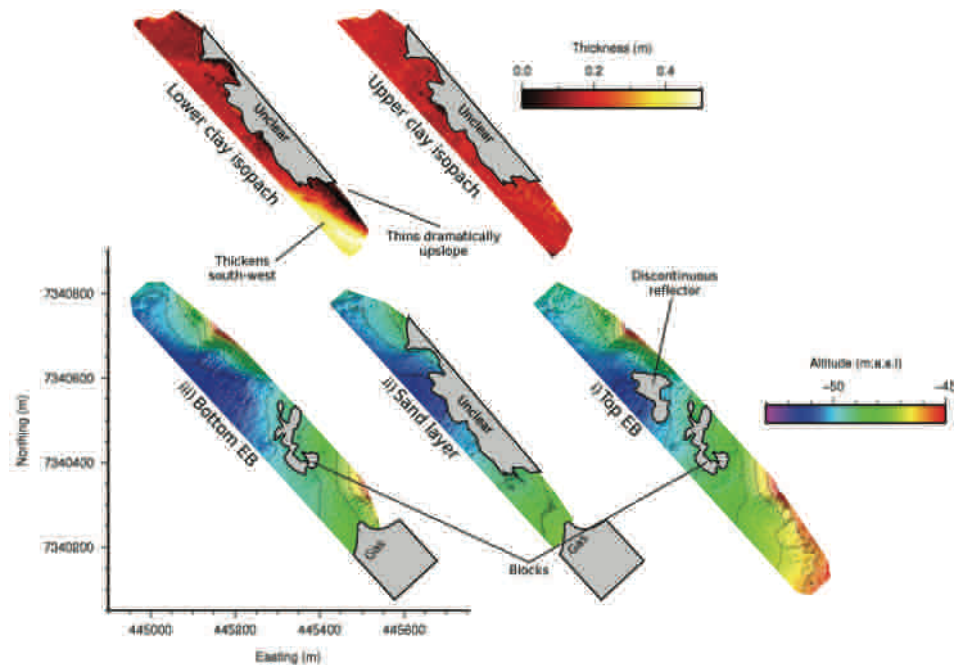

FIGURE 6
Surface maps as interpreted throughout the decimetre-resolution 3D seismic volume for (i) top reflection, (ii) sandy layer and (iii) base reflection of the event bed, together with isopach maps for upper and lower facies, which are representative of the morphology for upper and lower clay-rich layers. Areas of blanking by consolidated slide blocks and gas, together with deformation of top reflection are identified.
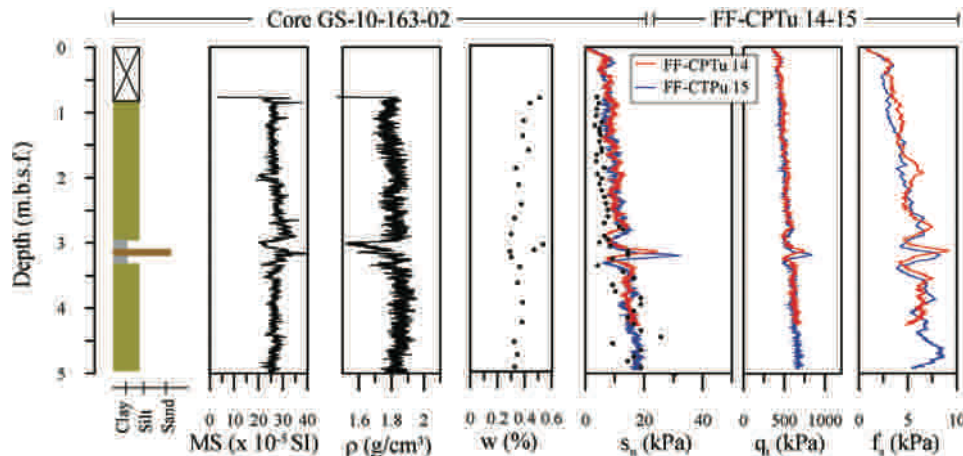

FIGURE 7
Sedimentological, magnetic susceptibility (MS), gamma density (ρ) and water content (w) core logs from piston core GS-10-163-02, together with undrained shear strength (s_u), total corrected cone resistance (q_t) and sleeve friction (f_s) from two coincident FF-CPTU profiles (FF-CPTU 14 and 15).
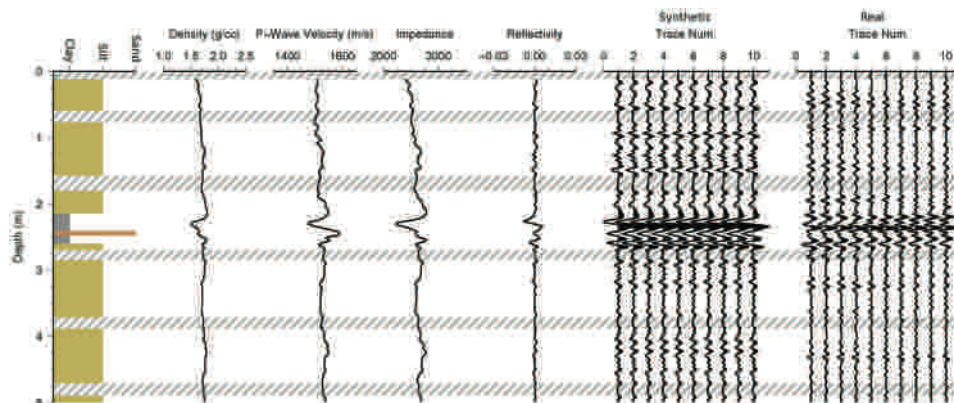

FIGURE 8
Sedimentological, gamma density and P-wave velocity logs from piston core GS-10-163-01, together with impedance, reflectivity and ten synthetic traces calculated using the core logs and theoretical Chirp waveform. For comparison, ten traces from the 3D seismic volume, centred on the core location, are shown. Note the depth values are relative to the top of the core.

Integration with soil properties

In Kullenberg-Calypso piston core GS-10-163-2, which is within the area covered by the 3D seismic volume but through undisturbed sediment immediately adjacent to the landslide deposit (Fig. 2), the sediment above and below the event bed is dominated by a homogenous, brownish, silty clay with some shell fragments. Only subtle variations in magnetic susceptibility, P-wave velocity and density logs occur (Fig. 7). These characteristics change suddenly at 2.9 m depth where the background sedimentation is interrupted by a 45 cm thick bed (the event bed), consisting of a 5 cm thick sand layer fining upwards sandwiched between two distinct grey clay-rich layers, both 20 cm thick (Fig. 7). This event bed is characterized by lows in both magnetic susceptibility and gamma-ray density that correspond to the two clay-rich layers and a very sharp peak in magnetic susceptibility and gamma-ray density for the sandy layer (Fig 7). *In situ* penetrometer tests also demonstrate that the event bed is a composite unit. The sandy unit is characterized by a positive peak in tip resistance, sleeve friction and a close-to-hydrostatic pore pressure response. The clay units surrounding the sand seam have low tip resistance, higher pore pressure response and markedly lower sleeve friction.

The water content for the background silty clay averages around 35% and varies only slightly throughout the fjord in other cores. In contrast, the water content is systematically higher in the event bed, typically in the range 45–65%. Undrained shear strength (s_u), determined from fall cone tests are typically lower for the event bed with values of 4–8 kPa, whereas the ratio of undrained shear strength and effective vertical stress (s_u/σ'_{v0}) falls between 0.2–0.3 (Fig. 7). In contrast, ratios for the background brownish silty sediments generally exceed 0.3. Shear strengths from *in situ* penetrometer tests compare well with the fall cone results (Fig. 7). In all analysed *in situ* tests, the cone resistance and sleeve friction are 1.5–2.0 times lower in the weak layers than in the surrounding sediments (see also, Steiner *et al*. 2012).

The depth of this event bed correlates well with the depth of the high-amplitude, composite reflection in the TOPAS and VHR3D data. Using V_p and density core logs from Kullenberg-Calypso piston core GS-10-163-1 and the known Chirp Klauder wavelet (Gutowski *et al*. 2002), a synthetic seismic trace was calculated for comparison with coincident traces extracted from the 3D seismic volume. Figure 8 compares a panel of ten synthetic traces with ten traces from the volume representing a 1.25 m window of traces centred on the core location (trace 6). The correlation in wavelet shape and peak polarities around the event bed is excellent. A distinct positive peak (i.e., reverse polarity reflection) corresponds to the top of the upper clay-rich layer, a negative peak (i.e., normal polarity) corresponds to the bottom of the lower clay-rich, while the negative peak of a complex wavelet approximately corresponds to the sandy layer. This result allows correlation of the three seismic reflections (i, ii and iii) described earlier as corresponding to: the top and bottom of the event bed (i and iii, respectively); and a composite wavelet (ii) formed by reflections from the top and bottom of the sandy

layer, which acts as a classical thin bed (e.g., Widess 1982). As such, the isopach maps for the upper and lower facies are representative of variations in thicknesses of the upper and lower clay-rich layers.
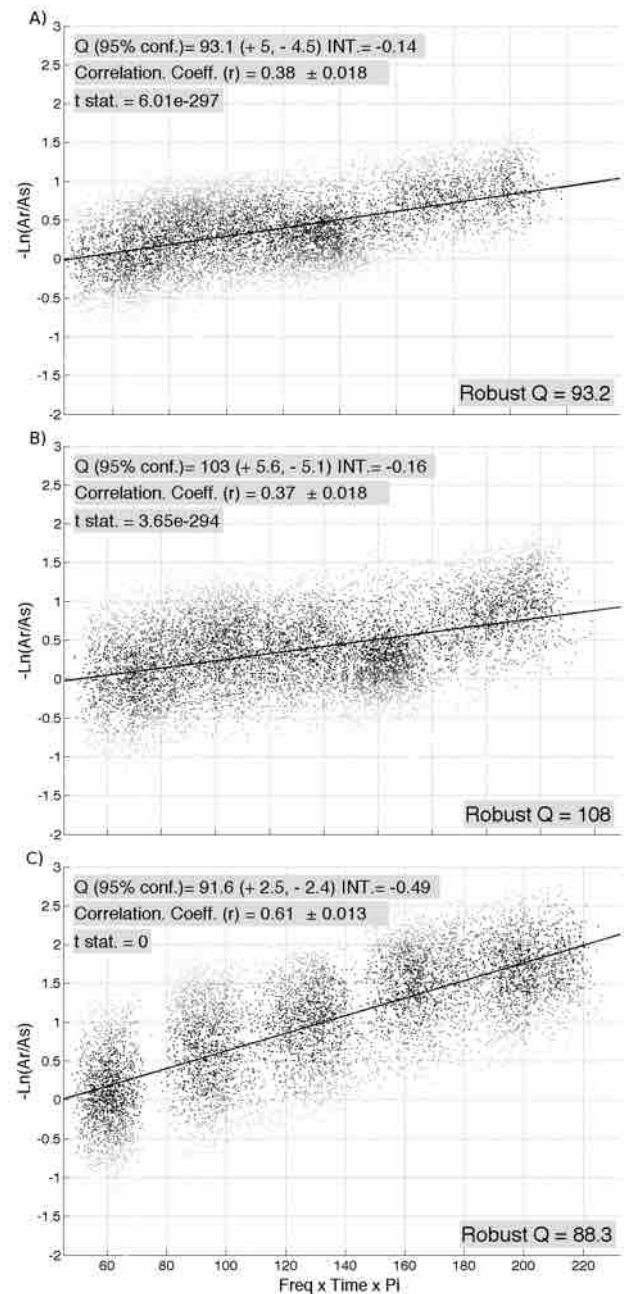

FIGURE 9

Plots of the fjord bed and subsurface reflection amplitude ratios against frequency multiplied by time and Pi using 7000 traces for: the top event bed (A); base event bed (B); and a deeper reflection (C). The gradients of these data are used to estimate robust *Q*-factors for the overlying sediments. The grey scale indicates the statistical weight of a data point when calculating robust regression, darker colours representing a stronger contribution (Pinson *et al*. 2008).
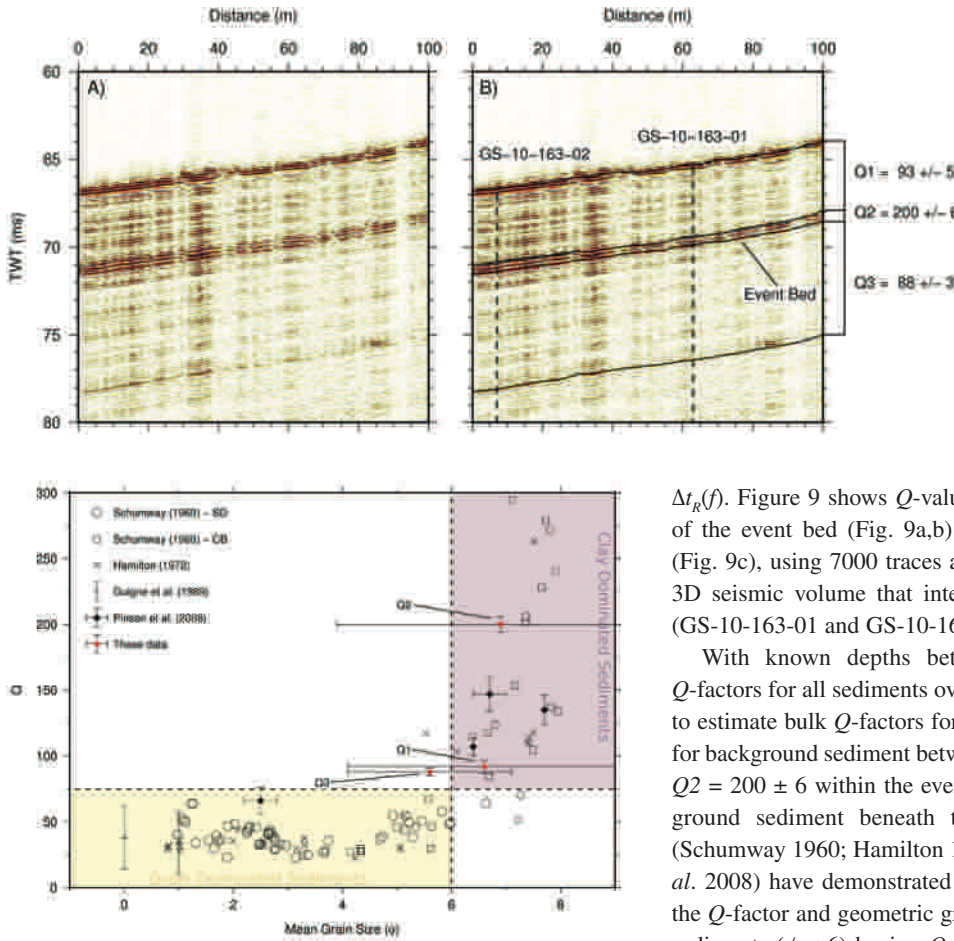
FIGURE 11

Empirical relationship between *Q* and grain size, combining data from Schumway (1960), Hamilton (1972), Guigné *et al.* (1989), Pinson *et al.* (2008) and these data. Image modified from Pinson *et al.* (2008).

Remote acoustic properties

Pinson *et al.* (2008) described a spectral-ratio method for calculating the acoustic quality factor (*Q*) from high-resolution seismic reflection data. In this method, the ratio between reflection amplitudes for the seafloor and a subsurface reflection are related to 1/*Q* for a series of frequency bands:

$$\ln\left|\frac{A_R(f)}{A_S(f)}\right| = \ln C - \frac{\pi \cdot f \cdot \Delta t_R(f)}{Q(f)} \qquad (1)$$

where $A_S(f)$ and $A_R(f)$ are amplitudes of the sea-bed and subsurface reflection at frequency *f*, $Q(f)$ is the quality factor for the sediment between the two reflections at frequency *f*, $\Delta t_R(f)$ is the two-way traveltime difference between the two reflections and *C* is a constant collecting together unknown terms (including spherical divergence and reflection coefficients for the two reflectors).

An average *Q* for a package of sediment between the seafloor and a sub-parallel subsurface reflection can be calculated by finding the gradient of data plotted as $-\ln[A_R(f)/A_S(f)]$ against $\pi.f.$

$\Delta t_R(f)$. Figure 9 shows *Q*-values calculated for the top and base of the event bed (Fig. 9a,b) together with a deeper reflection (Fig. 9c), using 7000 traces along a composite line through the 3D seismic volume that intersects both the long piston cores (GS-10-163-01 and GS-10-163-02).

With known depths between reflections, these average *Q*-factors for all sediments overlying each reflection can be used to estimate bulk *Q*-factors for each layer (Fig. 10): *Q1* = 93 ± 5 for background sediment between the seafloor and the event bed; *Q2* = 200 ± 6 within the event bed; and *Q3* = 88 ± 3 for background sediment beneath the event bed. Previous authors (Schumway 1960; Hamilton 1972; Guigné *et al.* 1989; Pinson *et al.* 2008) have demonstrated an empirical relationship between the *Q*-factor and geometric grain size (ϕ); with grain-dominated sediments ($\phi < 6$) having *Q* between 0–75 and clay-dominated sediments ($\phi > 6$) having *Q* > 75 (Fig. 11). Our calculated *Q* values can be combined with initial grain size measurements (red stars, Fig. 11). Despite the large error bars associated with the grain size measurements currently available, these data are in agreement with the sedimentological analysis.

DISCUSSION

The integration of geological and geophysical data indicates that the composite reflection, which correlates with the base of multiple landslide events in the Sørfjord region, comprises three sub-units; a thin (c. 5 cm) sandy unit sandwiched between two clay-rich units. In the decimetre-resolution geophysical data this composite manifests itself as three distinct reflections (the 5 cm sandy unit behaving as a classical thin bed), defining two sub-facies that are representative of the upper and lower clay-rich units. This regionally continuous layer is distinct from the background sedimentation of silty clays in terms of: grain size; density; water content; shear strength; and remote acoustic quality factor, *Q*.

Similar beds observed in other fjords around Norway (L'Heureux *et al.* 2009, 2010; Hansen *et al.* 2011) and Canada (St-Onge *et al.* 2004) were identified as being the result of terrestrial quick-clay landslides in the catchment of the fjord. Such events can produce a turbidity current that propagates down-

stream into the fjord, rapidly draping the fjord bed. Based on sedimentological analysis, L'Heureux *et al*. (2012) proposed a similar mechanism for the event bed in Sørfjord, identifying a large number of slide scars in the quick clay deposits either side of the Røssåga River.

The morphology and internal architecture of this event bed as imaged in the 3D seismic volume is consistent with this hypothesis. In particular, the manner in which the lower clay-rich layer demonstrates limited run-up on the foreshore slope and thickens south-west, toward the Røssåga River, agrees with the fine-grained, clay-rich gravity flow that is expected to form the first deposit in such an event (Hansen *et al*. 2011). The sandy interval may be associated with failure of the delta slope and/or flooding of the river (i.e., dam breach) following clay slide activity in the uplifted valley (L'Heureux *et al*. 2012). Meanwhile, the consistent thickness of the upper clay-rich layer agrees with the final stage of deposition for such models; gravitational settling of the clay-rich suspension plume, forming a consistent drape.

Specifically, in the case of the 1996 landslide near Finneidfjord, the identification and mapping of the three key reflectors (i, ii, iii) indicates that the glide plane for the 1996 landslide lies within the upper clay-rich layer. Confining the glide plane to the upper clay-rich layer agrees with the short cores higher up the foreshore slope that sample the exposed glide plane. In these cores, the sandy and lower clay-rich layers are preserved, while the upper clay-rich layer is still present but significantly thinner than observed in cores through immediately adjacent undisturbed material (L'Heureux *et al*. 2012). The preservation of some upper clay-rich material suggests that the 'weakness' of this layer is not a result of contrasts between the event bed and the overlying sediment but rather due to contrasts and/or mechanical properties within the event bed itself. While the physical properties of the event bed were shown, at this site and in other similar fjords, to be strongly dependent on the formation processes (i.e., rapid, almost catastrophic deposition of sensitive clay-rich material), it is unlikely that this alone makes the layer weak enough to fail. Instead, post-depositional factors such as shallow gas and/or fluid flow are likely to have played a role as well.

Although there is free gas present in the vicinity of the landslide, the 3D seismic volume confirms that the landslide deposit and the primary gas front are laterally separated by several hundred metres. This offset, together with the morphology of the landslide (which indicates initial failure higher up the foreshore slope), implies that landsliding was not directly related to gas associated with the gas front. Rather, the role of gas is likely to be limited to free gas observed as vesicles in split short cores acquired throughout the fjord (L'Heureux *et al*. 2012). These vesicles could be related to exsolution of gas from the pore waters upon retrieval of the core. Inversion of attenuation from airgun data in this area indicates that the gas saturation is very low, typically less than 0.15% (Morgan *et al*. In Press.). It is,

therefore, considered unlikely to significantly affect the *in situ* soil strength. Of the alternative hypothesis for increasing pore pressures within the event bed (excess sediment loading along the foreshore slope or artesian fluid flow), we favour the hypotheses presented by L'Heureux *et al*. (2012), that landsliding in Sørfjord and similar regions is strongly influenced by fluid flow, particularly groundwater.

CONCLUSIONS

- Using a combination of geophysical and geotechnical techniques, the event bed that coincides with the glide plane of multiple submarine landslides in the Sørfjord area was identified as a composite bed of three subunits; a thin sandy layer sandwiched between two clay-rich layers.
- This composite bed is distinct from the background sedimentation of silty clays in terms of: grain size; density; water content; shear strength; and remote acoustic quality factor, Q.
- The 3D morphology and stratification of the bed is consistent with originating as a terrestrial quick clay landslide in the fluvial catchment, as has been proposed for a number of similar sites in Norway.
- In the case of the 1996 landslide, the glide plane lies within the upper sub-unit of this event bed and may be strongly fluenced by groundwater artificially raising pore pressures.

REFERENCES

Best A.I., Clayton C.R.I., Longva O. and Szuman M. 2003. The role of free gas in the activation of submarine slides in Finneidfjord. In: *Submarine Mass Movements and their Consequences* (eds J. Locat and Mienert J.), pp. 491–498. Kluwer Academic Publishers, Dordrecht, Netherlands.

Bryn P., Berg K., Solheim K., Kvalstad T.J. and Forsberg C.F. 2005. Explaining the Storegga Slide. *Marine and Petroleum Geology* **22**, 11–19.

Bull J., Gutowski M., Dix J., Henstock T., Hogarth P., Leighton T. and White P. 2005. Design of a 3D Chirp sub-bottom imaging system. *Marine Geophysical Researches* **26**, 157–169.

Canals M., *et al*. 2004. Slope failure dynamics and impacts from seafloor and shallow sub- seafloor geophysical data: Case studies from the COSTA project. *Marine Geology* **213**, 9–72.

Gregersen O. 1999. Kvikkleireskredet i Finneidfjord 20 juni 1996. NGI Rep 980005–1, NGI, Oslo.

Guigné J.Y., Pace N.G. and Chin V.H. 1989. Dynamic extraction of sediment attenuation from subbottom acoustic data. *Journal of Geophysical Research* **94**, 5745–5755.

Gutowski M., Bull J.M., Dix J.K., Henstock T.J., Hogarth P., Hiller T. , Leighton T.G. and White P.R. 2008. 3D high-resolution acoustic imaging of the sub-seabed. *Applied Acoustics* **69**(5), 412–421.

Hamilton E. 1972. Compressional wave attenuation in marine sediments. *Geophysics* **37**, 620–646.

Hansen L., L'Heureux J.-S. and Longva O. 2011. Turbiditic, clay-rich event beds in fjord-marine deposits caused by landslides in emerging clay deposits – Palaeoenvironmental interpretation and role for submarine mass-wasting. *Sedimentology* **58**(4), 890–915.

Janbu N. 1996. Raset I Finneidfjord – 20 juni 1996. Unpublished expert's report prepared for the County Sheriff of Nordland. Report Number 1, Revision 1.

Kvalstad T.J., Andresen L., Forsberg C.F., Berg K., Bryn P. and Wangen M. 2005. The Storegga slide: Evaluation of triggering sources and slide mechanics. *Marine and Petroleum Geology* **22**, 245–256.

Lastras G., Canals M., Urgeles R., Hughes-Clarke J.E. and Acosta J. 2004. Shallow slides and pockmark swarms in the Eivissa Channel, western Mediterranean Sea. *Sedimentology* **51**,1–14

L'Heureux J.-S., Hansen L. and Longva O. 2009. Development of the submarine channel at the mouth of the Nidelva River, Trondheimsfjorden, Norway. *Marine Geology* **260**, 30–44.

L'Heureux J.-S., Hansen L., Longva O., Emdal A. and Grande L. 2010. A multidisciplinary study of submarine landslides at the Nidelva fjord delta, Central Norway – Implications for geohazards assessments. *Norwegian Journal of Geology* **90**, 1–20.

L'Heureux J.-S., *et al.* 2012. Identification of weak layers and their role for the stability of slopes at Finneidfjord, northern Norway. In: *Submarine Mass Movements and their Consequences, Advances in Natural and Technological Hazards Research* (eds Y. Yamada *et al.*), p. 31. Springer Science.

Longva O., Janbu N., Blikra L.H. and Boe R. 2003. The 1996 Finneidfjord slide: Seafloor failure and slide dynamics. In: *Submarine Mass Movements and their Consequences* (eds Locat J. and Mienert J.), pp. 531–538. Kluwer Academic Publishers, Dordrecht, Netherlands.

Lunne T., Robertson P.K. and Powell J.J.M. 1997. *Cone Penetration Testing In Geotechnical Practise*. p 312. Spon Press, Taylor & Francis Group, London and New York.

Masson D.G., Harbitz C.B., Wynn R.B., Pedersen G. and Løvholt F. 2006. Submarine Landslides – Processes, triggers and hazard prediction. *Philosophical Transactions of the Royal Society of London* A 364, 2009–2039.

Masson D.G., Wynn R.B. and Talling P.J. 2010. Large landslides on passive continental margins: Processes, hypotheses and outstanding questions. In: *Submarine Mass Movements and Their Consequences, Advances in Natural and Technological Hazards Research*, Vol. 28 (eds D.C. Mosher *et al.*). Springer Science.

Morgan E., Vanneste M., Lecomte I., Baise L.G., Longva O. and McAdoo B. Estimation of free gas saturation from seismic reflection surveys by the genetic algorithm inversion of a P-wave attenuation model. *In Press*, Geophysics.

Morgan E., Vanneste M., Longva O., Lecomte I., McAdoo B. and Baise L. 2009. Evaluating gas-generated pore pressure with seismic reflection data in a landslide-prone area: An example from Finneidfjord, Norway. In: *Submarine Mass Movements and Their Consequences, Advances in Natural and Technological Hazards Research*, Vol. 28 (eds D.C. Mosher *et al.*). Springer Science.

O'Leary D.W. 1991. Structure and morphology of submarine slab slides: Clues to origin and behavior. *Mar. Geotech.* **10**, 53–69.

Olsen L., Sveian H. and Bergstrom B. 2001. Rapid adjustments of the Western Part of the Scandinavian Ice Sheet during the Mid and Late Wiechselian: A new model. *Norsk Geologisk Tidsskrift* **81**, 93–118.

Olsen L., Sveian H. and Blikra L.H. 1996. KORGEN 1927 II. Quaternary map – M: 1:50 000, with description. Geological Survey of Norway.

Olsen L., Sveian H. and Vatne G. 2006. Trondheim Region Field Guide. ESF Sediflux and IAG/AIG Sedibud Excursion 01.11.2006, 24 pp.

Pinson L.J.W., Henstock T.J., Dix J.K. and Bull J.M. 2008. Estimating quality factor and mean grain size of sediments from high-resolution marine seismic data. *Geophysics* **73**(4), G19–G28.

Rosenquist I.T. 1953. Considerations on the sensitivity of Norwegian quick-clays. *Geotechnique* **3**, 195–200.

Shumway G. 1960. Sound speed and absorption studies of marine sediments by a resonance method. *Geophysics* **25**, 451–467.

Steiner A., L'Heureux J.S., Longva O., Lange M., Vanneste M., Haflidason H. and Kopf A. 2012. An in-situ free-fall piezocone penetrometer for characterizing soft and sensitive clays at Finneidfjord, northern Norway. In: *Submarine Mass Movements and Their Consequences, Advances in Natural and Technological Hazards Research*, 29 (eds Y. Yamada *et al.*). Spinger, Dordrecht (The Netherlands).

St-Onge G., Mulder T., Piper D.J.W., Hilaire-Marcel C. and Stoner J.S. 2004. Earthquake and flood-induced turbidites in the Saguenay Fjord (Québec): A Holocene paleoseismicity record. *Quaternary Science Reviews* **23**, 283–294.

Vanneste M., L'Heureux J.-S., Brendryen J., Baeten N., Laberg J.S., Vardy M.E. *et al.* 2012. Assessing offshore geohazards: A multi-disciplinary research initiative to understand shallow landslides and their dynamics in coastal and deepwater environments, Norway. In: *Submarine Mass Movements and Their Consequences, Advances in Natural and Technological Hazards Research*, 29 (eds Y. Yamada *et al.*). Spinger, Dordrecht, The Netherlands.

Vardy M.E., Bull J.M., Dix J.K., Henstock T.J., Plets R.M.K., Gutowski M. and Hogarth P. 2011. The geological 'Hubble': A reappraisal for shallow water. *The Leading Edge* (**2**), 154–159.

Vardy M.E. and Henstock T.J. 2010. A frequency approximated approach to Kirchhoff migration. *Geophysics* **75**(6), S211–S218.

Vardy M.E., Pinson L.J.W., Bull J.M., Dix J.K., Henstock T.J., Davis J.W. and Gutowski M. 2010. 3D seismic imaging of buried Younger Dryas mass movement flows: Lake Windermere, UK. *Geomorphology* **118**(1–2), 176–187.

Widess M.B. 1973. How thin is a thin bed? *Geophysics* **38**, 1176–1180.

Wilson C.K., Long D. and Bulat J., 2004. The morphology, setting and processes of the Afen slide. *Marine Geology* **213**, 149–167.